A EUROPEAN JOURNAL

CHEMPHYSCHEM

OF CHEMICAL PHYSICS AND PHYSICAL CHEMISTRY

Accepted Article

Title: Unveiling the Photo- and Thermal-Stability of Cesium Lead Halide Perovskite Nanocrystals

Authors: Brett W. Boote, Himashi P. Andaraarachchi, Bryan A. Rosales, Rafael Blome-Fernández, Feng Zhu, Malinda D. Reichert, Kalyan Santra, Jingzhe Li, Jacob W. Petrich, Javier Vela, and Emily A. Smith

To be cited as: *ChemPhysChem* 10.1002/cphc.201900432

Link to VoR: http://dx.doi.org/10.1002/cphc.201900432

A Journal of

ChemPubSoc Europe

WILEY-VCH

www.chemphyschem.org

Unveiling the Photo- and Thermal-Stability of Cesium Lead Halide Perovskite Nanocrystals

Brett W. Boote,[a,b] Himashi P. Andaraarachchi,[a,b] Bryan A. Rosales,[a] Rafael Blome-Fernández,[a] Feng Zhu,[a] Malinda D. Reichert,[a] Kalyan Santra,[a,b] Jingzhe Li,[a,b] Jacob W. Petrich,[a,b] Javier Vela,[a,b,*] Emily A. Smith [a,b,*]

Affiliations

[a]Department of Chemistry, Iowa State University, and [b]Ames Laboratory, U.S. Department of Energy, Ames, Iowa 50011-3111, United States

Abstract

Lead halide perovskites possess unique characteristics that are well-suited for optoelectronic and energy capture devices, however, concerns about their long-term stability remain. Limited stability is often linked to the methylammonium cation, and all-inorganic $CsPbX_3$ (X = Cl, Br, I) perovskite nanocrystals have been reported with improved stability. In this work, the photostability and thermal stability properties of $CsPbX_3$ (X = Cl, Br, I) nanocrystals were investigated via electron microscopy, x-ray diffraction, thermogravimetric analysis coupled with FTIR (TGA-FTIR), ensemble and single particle spectral characterization. $CsPbBr_3$ was found to be stable under 1-sun illumination for 16 h in ambient conditions, although single crystal luminescence analysis after illumination via a solar simulator indicates that the luminescence states are changing over time. $CsPbBr_3$ was also stable to heating to 250 °C. Large $CsPbI_3$ crystals (34 ± 5 nm) were shown to be the least stable composition under the

same conditions as both XRD reflections and Raman bands diminish under irradiation; and with heating the γ (black) phase reverts to the non-luminescent δ phase. Smaller $CsPbI_3$ nanocrystals (14 ± 2 nm) purified by a different washing strategy exhibited improved photostability with no evidence of crystal growth but were still thermally unstable. Both $CsPbCl_3$ and $CsPbBr_3$ show crystal growth under irradiation or heat, likely with a preferential orientation based on XRD patterns. TGA-FTIR revealed nanocrystal mass loss was only from liberation and subsequent degradation of surface ligands. Encapsulation or other protective strategies should be employed for long-term stability of these materials under conditions of high irradiance or temperature.

Keywords

Lead halide perovskites, photostability, degradation, semiconductor nanocrystals, single crystal luminescence

[a] Dr. B. W. Boote, Dr. H. P. Andaraarachchi, Dr. B. A. Rosales, Mr. R. Blome-Fernández, Dr. F. Zhu, Dr. M. D. Reichert, Mr. K. Santra, Ms. J. Li, Prof. Dr. J. W. Petrich, Prof. Dr. J. Vela,* Prof. Dr. E. A. Smith*

Department of Chemistry, Iowa State University, Ames, Iowa 50011, United States

E-mail: esmith1@iastate.edu, vela@iastate.edu

[b] Dr. B. W. Boote, Dr. H. P. Andaraarachchi, Mr. K. Santra, Ms. J. Li, Prof. Dr. J. W. Petrich, Prof. Dr. J. Vela,* Prof. Dr. E. A. Smith*

The Ames Laboratory, U.S. Department of Energy, and Department of Chemistry, Iowa State University, Ames, Iowa 50011, United States

E-mail: esmith1@iastate.edu, vela@iastate.edu

Supporting information for this article is given via a link at the end of the document.

ARTICLE

Brett W. Boote, Himashi P. Andaraarachchi, Bryan A. Rosales, Rafael Blome-Fernández, Feng Zhu, Malinda D. Reichert, Kalyan Santra, Jingzhe Li, Jacob W. Petrich, Javier Vela, Emily A. Smith**

Page No. – Page No.

Unveiling the Photo- and Thermal-Stability of Cesium Lead Halide Perovskite Nanocrystals

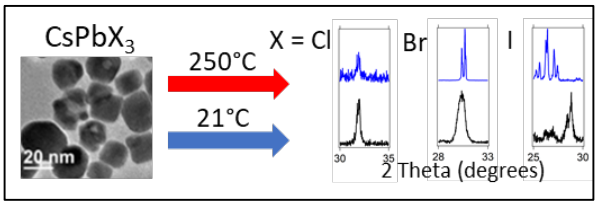

The photophysical properties of cesium lead halide nanocrystals show great promise in derived devices due to high quantum yields and tunable visible photoluminescence, but stability concerns remain. In this work, the photostability and thermal stability of cesium lead halide nanocrystals were investigated using a combination of X-ray diffraction, Raman spectroscopy, single crystal luminescence imaging, and thermal gravimetric analysis. The observed changes in the nanocrystals as a result of illumination and heating were found to be highly dependent on halide composition.

Introduction

The unique photophysical properties and straightforward synthesis of perovskite-based materials make them promising materials for solar energy applications.[1-4] The first-generation methylammonium lead halide ($MAPbX_3$) perovskites have been shown to degrade rapidly when exposed to ambient conditions with moderate humidity,[5] which led to the increased study of new compositions such as the all-inorganic cesium lead halide ($CsPbX_3$) perovskites. $CsPbX_3$ nanocrystals have been incorporated into solar cells achieving a record 13.4% power conversion efficiency (PCE).[6-10] In addition to light absorption or conversion for energy capture, these materials have been reported for possible use in laser media,[11-14] LEDs,[15-18] and photodetectors.[12, 19-20]

Most reported syntheses of $CsPbX_3$ follow the work of Protesescu *et al*. who demonstrated a simple, solution-based synthesis for nanocrystals with high luminescence.[15] Other syntheses have expanded this general idea by generating multiple nanocrystal morphologies through ligand mediation[21-22] and reaction tuning,[23] by using different surface ligands for improved quantum yields,[24-25] by increasing surface passivation/repair via salt solutions,[26-29] as well as by generating other cation/anion compositions through doping[17, 30-35] or post-synthetic ion exchange.[19, 22, 36-39] In addition, triple-cation (Cs,formamidinium,methylammonium)PbX_3 materials have been developed with the goal of increasing stability while maintaining bright luminescence.[26, 40]

The photophysics of $MAPbX_3$ nanocrystals have been extensively studied,[41-50] and there are several reports on various luminescence properties of $CsPbX_3$.[51-54] Park *et al*. observed strong photon antibunching as well as blinking behavior ascribed to charge/discharge events triggered by photoionization in $CsPbBr_3$ and $CsPbI_3$.[52] Recently, Becker *et al*. showed

the lowest triplet exciton for $CsPbX_3$ is bright, which explains the anomalously fast emission rates for these materials compared to other semiconductors.[55] Pan *et al*. first demonstrated lanthanide doping into $CsPbCl_3$, showing improved quantum yield and luminescence bands across the visible and even into the near-IR region.[56] Both transition metals[35, 57] and rare earth metals[34] have been doped into $CsPbX_3$, achieving quantum yields greater than 60% and 170%, respectively. Beimborn *et al*. studied the effect of pressure-induced deformation on the photoluminescence, which leads to a fully reversible blue shift with decreasing intensity.[58] Raino and coworkers observed suppressed blinking and a fast decay from low-temperature (6 K) photoluminescence measurements of $CsPbCl_xBr_{3-x}$ nanocrystals.[53] In contrast, Diroll *et al*. studied high temperature photoluminescence of $CsPbX_3$ nanocrystals (up to 550 K), showing reversible photoluminescence loss below 450 K for $CsPbBr_3$ (the highest threshold among the compositions studied).[51]

Since $CsPbX_3$ materials have considerable potential for use in functional devices, the stability of their nanocrystals is of utmost importance. $CsPbCl_3$ and $CsPbBr_3$ nanocrystals are reported to be stable in the cubic phase, while $CsPbI_3$ slowly reverts to the thermodynamically-favored δ-phase, which is yellow.[15] This phase change is accelerated with harsh washing reagents and, with a more gentle washing strategy—using methyl acetate or MeOAc—$CsPbI_3$, is stable in the γ (black) phase for over 2 months.[59] Importantly, the δ phase for $CsPbI_3$ is non-luminescent, rendering the material unusable for most applications. Park *et al*. observe a 16-nm blue shift and eventual degradation in $CsPbI_3$ nanocrystals that were caused by the irreversible generation of surface defects during photoluminescence measurements.[52] Liu and coworkers compare $CsPbI_3$ nanocrystals stabilized with trioctylphosphine (TOP) to those stabilized with oleic acid and oleylamine.[24] They found the TOP-stabilized nanocrystals show improved

quantum yield, and are stable for at least one month under ambient conditions. When dry films of the nanocrystals are prepared, however, the common δ-$CsPbI_3$ phase transition is observed after 3 days. Yuan *et al*. demonstrated that $CsPbI_3$ nanocrystals undergo irreversible photodegradation that quenches the photoluminescence under light irradiation.[54] For films in air, photobrightening followed by photodegradation was observed under illumination, and degradation is also observed for films in dark, ambient conditions. Additionally, several groups have been developing methods of protecting the perovskite structure from moisture, including overlaying silicone resins,[60] preparing polymer or related composites,[61-63] and coating with zwitterion[64] or metal complexes.[17, 65]

A recent report by Liao *et al*. describes the thermal stability of cesium lead halide perovskites from -190 to 500 °C using Raman spectroscopy and XRD.[66] They found that $CsPbCl_3$ nanocrystals were the most thermally stable among (X=Cl, Br, I) compositions, as $CsPbBr_3$ and $CsPbI_3$ nanocrystals decomposed at ~400 and 200 °C, respectively. Though several stability studies have been performed on $CsPbX_3$ nanocrystals, as well as their derived devices,[67] to the best of our knowledge a fundamental study describing how the halide composition of the perovskites affects the photostability and photophysical states of the nanocrystals has not yet been performed. With this work, we set out to understand the connection between the photophysical properties of the $CsPbX_3$ perovskite materials and their stability under conditions likely encountered in many applications, namely light irradiance and thermal stress.

Results and Discussion

General Characterization and Photophysical Properties of $CsPbX_3$ Nanocrystals

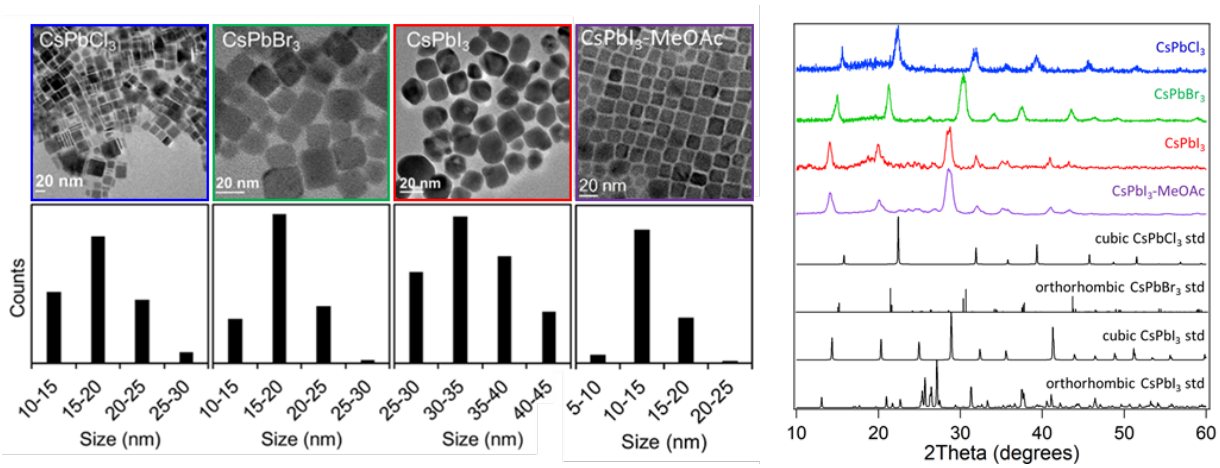

Figure 1. TEM images, size histograms, and XRD patterns for cesium lead perovskite nanocrystals.

Cesium lead halide perovskite nanocrystals were prepared via a modified literature method[15] with the goal of understanding their photophysical properties as well as their photostabilty and thermal stability. **Figure 1** shows electron microscopy images, size histograms, and XRD patterns for the cesium lead halide nanocrystals. In general, the nanocrystals exhibit cubic morphology, although the $CsPbCl_3$ sample also showed evidence of platelets/stacking. When using identical synthetic conditions, the $CsPbI_3$ sample always formed larger nanocrystals than the other compositions after washing with acetone/methanol. The sizes of the nanocrystals washed with acetone/methanol were 17 ± 3 nm for $CsPbCl_3$, 17 ± 4 nm for $CsPbBr_3$, and 34 ± 5 nm for $CsPbI_3$. The size difference should not have a pronounced effect on the nanocrystal photophysics as all of these sizes are above the Bohr radii for $CsPbX_3$ nanocrystals. In an effort, however, to isolate $CsPbI_3$ nanocrystals of a smaller size, another sample of crystals was washed with methyl acetate. The methyl acetate washed $CsPbI_3$ nanocrystals had a size of 14 ± 2 nm, similar to the acetone/methanol washed $CsPbCl_3$ and $CsPbBr_3$ nanocrystals.[59] While the size of the nanocrystals are similar, the surface chemistry can vary due to the different wash procedures, thus becoming another variable that may affect the photophysics and stability. For clarity, the methyl acetate washed sample will be labeled $CsPbI_3$-MeOAc. The TEM images of $CsPbI_3$-

MeOAc show nearly ideal cubic morphologies, which is consistent with highly crystalline surfaces. The XRD patterns of the nanocrystals are consistent with cubic standard patterns, although previous work on $CsPbX_3$ nanocrystals using Rietveld refinement has shown the PbX_6 octahedra can undergo dynamic distortions and rotations that lead to disorder and a resultant orthorhombic γ-phase for both $CsPbBr_3$ and $CsPbI_3$.[68-69]

Solution absorption and photoluminescence spectra for the nanocrystals are shown in **Figure 2**. The photoluminescence λ_{max} data are consistent with literature values for these materials and are 413, 523, 698, and 687 nm for $CsPbCl_3$, $CsPbBr_3$, $CsPbI_3$, and $CsPbI_3$-MeOAc, respectively.[15] Photoluminescence decay curves (**Figure S1**) yield average lifetimes for $CsPbCl_3$, $CsPbBr_3$, and $CsPbI_3$ of 1.2, 2.3, and 41.5 ns, respectively (the $CsPbI_3$-MeOAc sample was not measured). These values are consistent with previous reports,[15] although the $CsPbI_3$ sample showed a slightly longer lifetime, which is likely due to a larger average crystal size for the $CsPbI_3$ nanocrystals.

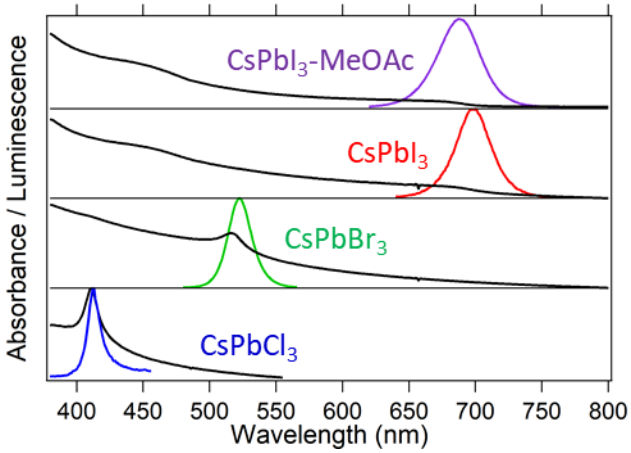

Figure 2. Solution absorption (black) and photoluminescence (color) spectra of the $CsPbX_3$ nanocrystals. The full width at half maximum values were 13, 22, 33, and 40 nm for $CsPbCl_3$, $CsPbBr_3$, $CsPbI_3$, and $CsPbI_3$-MeOAc, respectively.

To assess the photophysics of the perovskite nanocrystals further, single particle luminescence data were recorded for individual $CsPbBr_3$, $CsPbI_3$, and $CsPbI_3$-MeOAc

nanocrystals. For the $CsPbCl_3$ sample, the signal-to-noise ratio (SNR) was too low for quantification of the luminescence from single crystals, as shown by representative images from luminescence movies (**Figure S2**). This could be due to the presence of platelets in this sample, which has been shown to lead to more defects within the material due to a high surface area, and thus lower luminescence intensity.[70] The photoluminescence traces for $CsPbBr_3$, $CsPbI_3$ and $CsPbI_3$-MeOAc nanocrystals were categorized into constant- (intensity not significantly changing), photobleaching- (decreasing intensity), photobrightening- (increasing intensity), and bimodal- (two distinct intensity levels) luminescence types. Full information on the categories and mathematical treatment is available in Supporting Information, with resultsshown in **Figure S3**. In general, the nanocrystals from each halide composition spend the majority of the time in the ON state, regardless of luminescence type. The $CsPbBr_3$, $CsPbI_3$, and $CsPbI_3$-MeOAc nanocrystals were on for 87%, 97%, and 99% of the total analysis time, respectively. However, the populations of constant-, photobleaching-, photobrightening-, and bimodal-PL nanocrystals for the same compositions were approximately 4:2:1:1 (Br), 2:2:2:1 (I), and 5:18:1:1 (I-MeOAc) as shown in **Table S1**. Thus, while the $CsPbBr_3$ nanocrystals spend, on average, less total time in the ON state, there is a higher population of nanocrystals with stable luminescence when compared to the iodide-containing samples. $CsPbI_3$ nanocrystals showed similar populations of constant-, photobleaching-, and photobrightening-PL, whereas the $CsPbI_3$-MeOAc nanocrystals showed the highest tendency for photobleaching and had smaller populations with photobrightening- or bimodal-PL behavior. In a previous study on $CH_3NH_3PbI_3$ nanocrystals, photobleaching was the most common luminescence type observed, and this was attributed to increased non-radiative recombination events as a result of the breakdown of the crystal lattice at the surface.[42]

From the single crystal luminescence data, ON-OFF event histograms were extracted and fit to a power law decay and to a 3-exponential decay, using a maximum likelihood method. Maximum likelihood method was used because it has been shown to provide more accurate fit values when compared to residual minimization in sparse data sets.[71] The results of the ON-OFF fitting are shown in **Figure 3**, and the fit parameters are listed in **Table S1.** Tabulating histograms for single nanocrystals (267 for $CsPbBr_3$, 233 for $CsPbI_3$, and 250 for $CsPbI_3$-MeOAc), the most ON/OFF events were recorded for $CsPbBr_3$ nanocrystals, which had approximately 8× and 50× more total events than those recorded for $CsPbI_3$ and $CsPbI_3$-MeOAc, respectively. This indicates a higher probability of non-radiative recombination centers as a result of surface defects in the $CsPbBr_3$ sample. Interestingly, $CsPbI_3$-MeOAc nanocrystals have the longest lived ON state, and very few recorded OFF events. This is likely due to high crystallinity and reduced surface defects (as shown by near ideal cubic morphologies in TEM images). Comparing the power law and multi-exponential fits, the power law did not produce a good fit for the $CsPbI_3$ and $CsPbI_3$-MeOAc ON events, whereas the multi-exponential fit shows the tailing (to shorter durations) of the longer lived events. This observation is reminiscent of previous work showing events with longer ON times deviate from power law fits for $CsPbI_3$ nanocrystals.[52] Also, $CsPbI_3$ ON events are longer lived than $CsPbBr_3$, while the OFF states have a similar average duration.

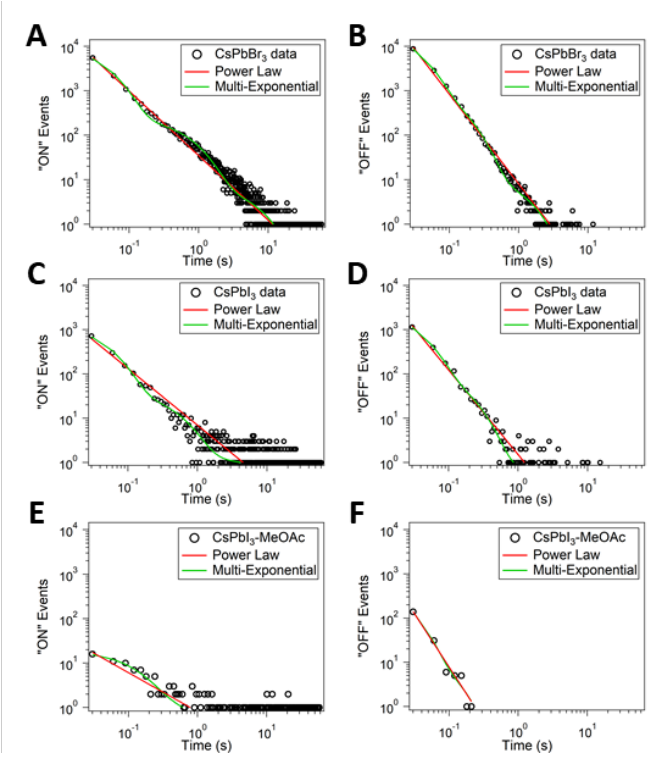

Figure 3. ON-OFF histogram plots of (A, B) $CsPbBr_3$, (C, D) $CsPbI_3$, and (E,F) $CsPbI_3$-MeOAc nanocrystals, based on analysis of 267, 233, and 250 nanocrystals, respectively. The data were fit using maximum likelihood estimation to a power law and a 3-exponential to better fit the non-Gaussian distributions of states.

Photostability of $CsPbX_3$ Nanocrystals

To assess nanocrystal photostability, a solar simulator was used to illuminate drop cast nanocrystal films under ambient conditions. XRD patterns of the samples after 2, 4, and 16 h of illumination are shown in **Figure 4**. Also, as a control experiment, a set of samples of each halide composition was kept in the dark under ambient conditions (**Figure S4**), which showed no structural changes over 16 h. $CsPbBr_3$ and $CsPbCl_3$ nanocrystals showed enhancement of the (100) and (200) planes, indicating possible orientation effects or anisotropic crystal growth under illumination. Crystal growth is also supported by a decrease in the width of the reflections, which is most evident for the $CsPbBr_3$ sample after 2 h of illumination. The apparent increase in crystal size is enough to elucidate the orthorhombic character of the nanocrystals as seen in the resolved

peaks at 15 and 15.2° 2θ, and at 30.4 and 30.7° 2θ. The $CsPbI_3$ nanocrystals showed significant loss of nearly all reflections after 16 h illumination, indicative of sample degradation into non-crystalline products. Interestingly, the $CsPbI_3$-MeOAc sample does not show signs of crystal growth and retains all major reflections of the γ-phase. This indicates that their more ideal crystalline surface improves the photostability of the nanocrystals.

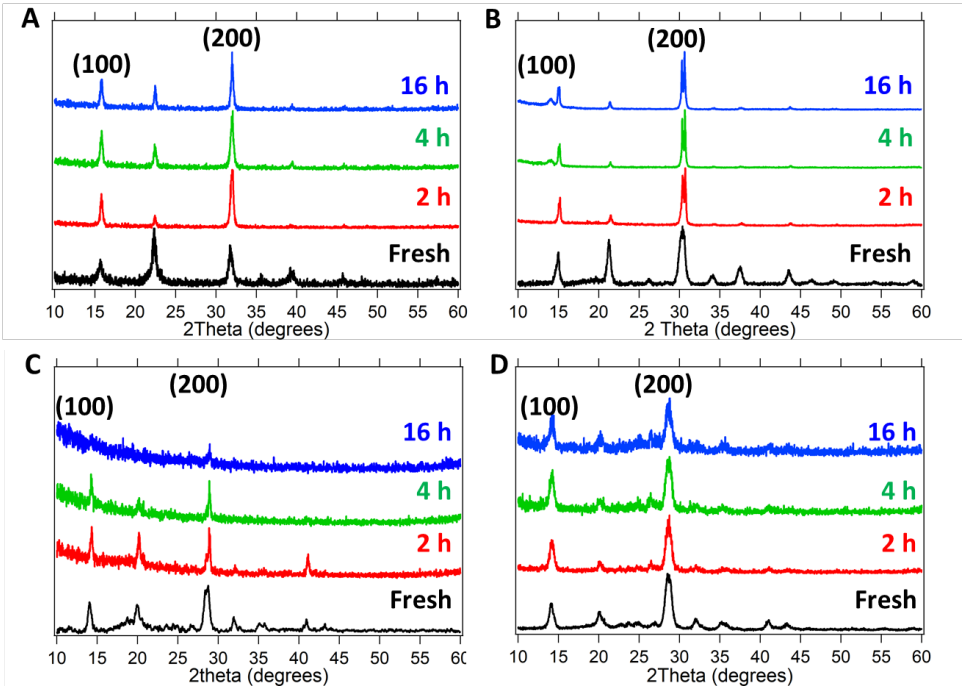

Figure 4. XRD patterns of A) $CsPbCl_3$, B) $CsPbBr_3$, C) $CsPbI_3$, and D) $CsPbI_3$-MeOAc nanocrystals before (fresh) and after exposure to a solar simulator from 2-16 h.

The XRD results are supported by Raman measurements of samples after solar simulator exposure (**Figure S5**). The nanocrystals of different halide compositions have similar Raman spectra, with one main band between 50 and 120 cm^{-1} and a broad response extending to ~200 cm^{-1}. This single broad band (as opposed to sharp, well-defined bands commonly observed in Raman spectra) is likely due to dynamic disorder within the nanocrystals at room temperature.[72] The Raman band intensity increases for both $CsPbCl_3$ and $CsPbBr_3$ up to 120 min of solar simulator exposure, which is consistent with the XRD patterns indicating crystal

growth. $CsPbI_3$ is the only sample that degrades over time with solar simulator exposure based on the Raman spectrum.

To decouple the synergistic effect of ambient moisture combined with light illumination on the nanocrystal stability, experiments were carried out using $CsPbI_3$-MeOAc nanocrystals illuminated with the solar simulator in a glove box under moisture-free conditions. The results are shown in the Supporting Information (S.I.) file. Comparing the results to ambient conditions, little to no effect on the photostability is attributed to the ambient moisture.

To monitor the effect of illumination on the photophysical states of the nanocrystals, single crystal luminescence movies were collected on diluted samples after 2 and 4 h of illumination by the solar simulator. The histograms are shown in **Figure 5**, with fit statistics shown in **Table S2**. The $CsPbBr_3$ sample showed the most significant change after light exposure; ON events were both fewer in number and much shorter in duration. Likewise,

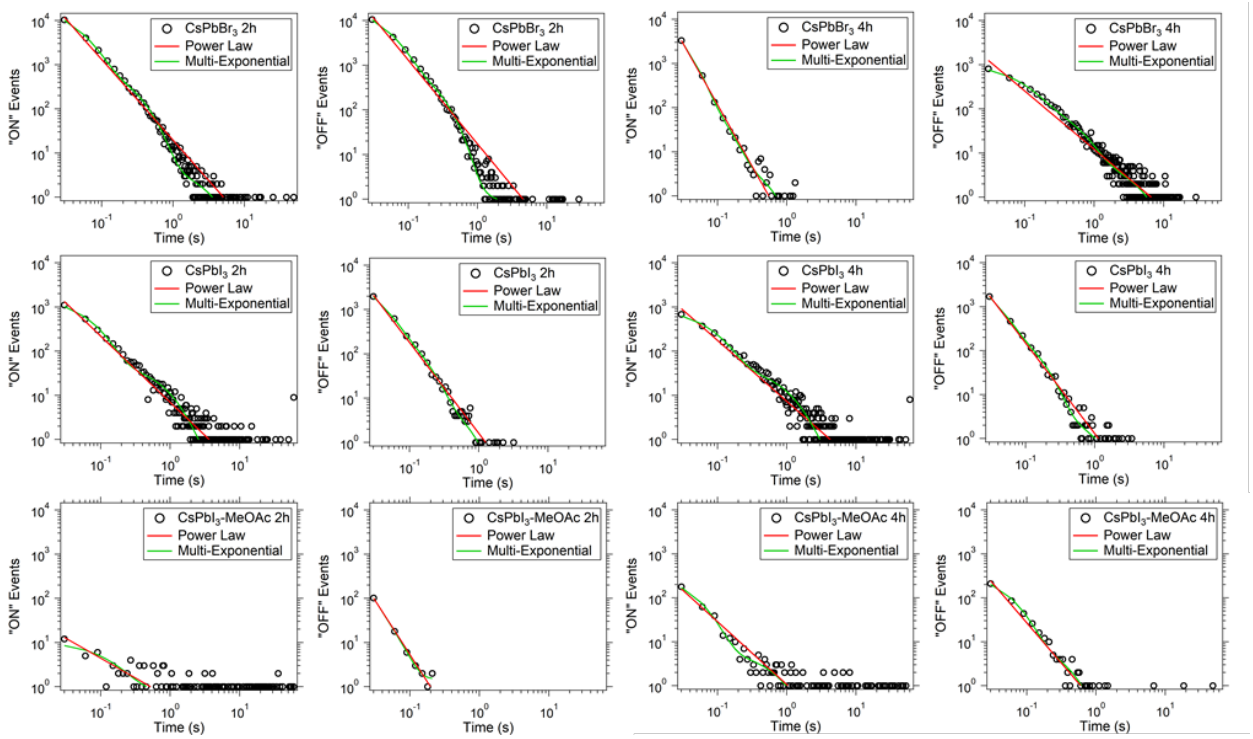

Figure 5. ON-OFF histograms of $CsPbBr_3$, $CsPbI_3$, and $CsPbI_3$-MeOAc nanocrystals following solar simulator exposure for 2 and 4 h. In all samples a minimum of 40 nanocrystals were analyzed to generate the histograms.

OFF events for this sample trended toward longer times while also decreasing in number of occurrences. For the $CsPbI_3$ sample, the ON-OFF histograms after 2 and 4 h solar simulator exposure show very similar characteristics in both number of events and trends for fit parameters, with only slight increases in longer lived states. Thus, while XRD shows the material eventually degraded after 16 h, the photophysical states do not appear to change over the first 4 h. For the $CsPbI_3$-MeOAc sample, which exhibited few ON-OFF events prior to illumination, the ON-OFF histograms after 2 and 4 h solar simulator exposure show steadily increasing numbers of ON-OFF events, especially OFF events with longer durations. Combining the results from all photostability experiments, the $CsPbBr_3$ and $CsPbI_3$-MeOAc nanocrystals both undergo changes in their luminescence states over time, which is one measure of photo-instability.

Thermal Stability of $CsPbX_3$ Nanocrystals

Even though the photostability is critically important for these materials in downstream applications, for many applications the thermal stability is important as well. In an effort to elucidate the thermal stability and compare to the photostability data of these nanocrystals, thermal stability measurements were performed. A temperature-controlled stage was used to expose drop-cast samples of nanocrystals to elevated temperatures after purging with nitrogen, and then XRD patterns were collected. The XRD patterns for the $CsPbX_3$ perovskite nanocrystals after heating are shown in **Figure 6**. For the three halide compositions, there are three different outcomes as a result of elevated temperatures. $CsPbCl_3$ nanocrystals initially show crystal growth up to 100 °C but show signs of degradation at 250 °C based on the SNR of the XRD pattern. While the cubic phase appears to be degrading, the identity of the degradation product(s) is not revealed by XRD. $CsPbBr_3$ nanocrystals show similar behavior to the

photostability measurements upon heating, that is crystal growth leads to a decrease in the width of the reflections and a clear orthorhombic pattern emerges. The crystal structure persisted even up to 250 °C. On the other hand, $CsPbI_3$ nanocrystals undergo a structural change beginning at 50 °C showing a transition from the luminescent γ-phase to a combination of PbI_2 and δ-phase $CsPbI_3$ (which is yellow in color, non-luminescent and thus not viable for devices). By 250 °C, the phase change is essentially complete, and there is a loss of all γ-phase reflections. It is known that the δ-phase is thermodynamically favored,[73] so this result makes sense at the elevated temperature. The $CsPbI_3$-MeOAc sample undergoes a very similar structural change from the γ-phase to the δ-phase above 100 °C. Both $CsPbI_3$ samples show reflections from PbI_2. Dastidar *et al*. showed $CsPbI_3$ is stable in the cubic phase up to 100 °C in a dry environment, thus our results confirm atmospheric moisture combined with heating accelerate the δ-phase transition.[74] Compared to the samples studied by Liao *et al*. wherein no crystal growth was reported, our $CsPbI_3$ and $CsPbI_3$-MeOAc samples underwent phase changes at lower temperatures and exhibited crystal growth. As with the photostability study, a sample of $CsPbI_3$-MeOAc nanocrystals was heated under moisture-free conditions using a glove box. The results are shown in S.I. file. The degradation pattern is the same at 250°, showing a combination of PbI¬2 and δ-phase reflections. In the ambient measurement, a partial degradation was observed at 100 °C while no degradation was observed in the moisture-free sample. Thus, moisture does not alter the degradation process but may change the temperature of degradation onset. With the exception of $CsPbI_3$, no clear degradation products are observed in the XRD patterns, so other complementary analysis techniques were employed to explore the possible products of thermal stress.

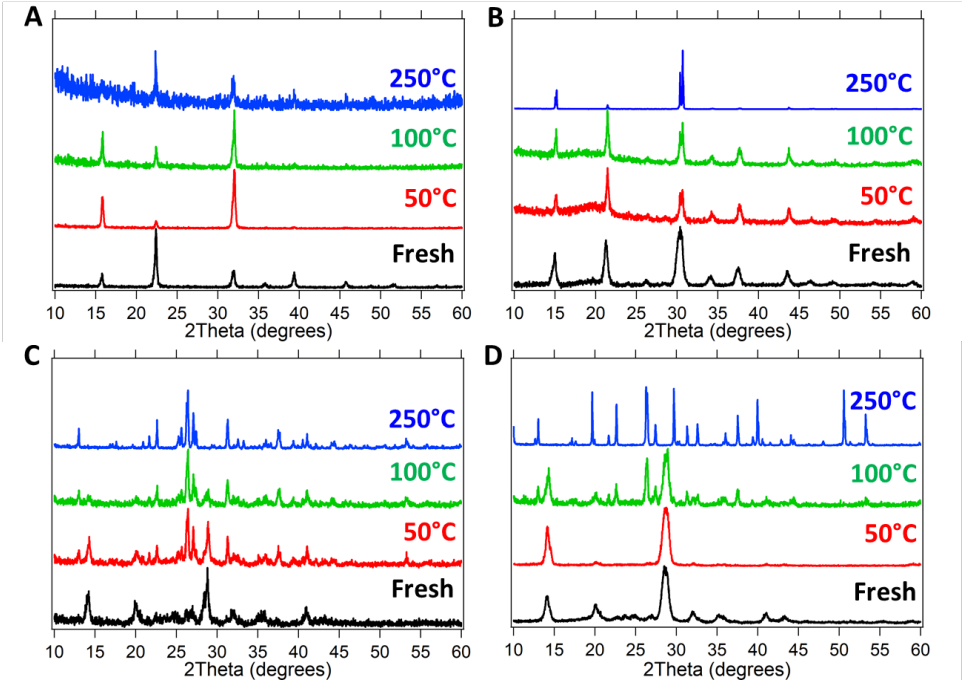

Figure 6. XRD patterns of A) $CsPbCl_3$ B) $CsPbBr_3$ and C) $CsPbI_3$ and D) $CsPbI_3$-MeOAc nanocrystals following exposure to the elevated temperatures shown.

Raman spectra were acquired for each halide composition at room temperature (21 °C) and then after heating to 250 °C and cooling back to room temperature (**Figure 7**). The high temperature spectra are not shown as the high kinetic energy produces a high background that obscures the Raman signal for all samples. Importantly, $CsPbI_3$ is the only sample that does not recover the original band structure, which would be consistent with XRD results if the δ-phase has a lower Raman cross section than the γ-phase. The other halides show similar spectra before and after heating, with a slight increase in the band around ~120 cm^{-1} for $CsPbBr_3$. For $CsPbCl_3$, it is curious that the Raman spectrum is retained after heating but the sample appears to be partially degraded in the XRD results. This could be due to the difference in sampling between these techniques: XRD probes a large sample area, whereas Raman spectroscopy is collected on small aggregates that are visible in the microscope image. If the sample degradation starts with

single crystals (and there is minimal degradation of aggregates), the Raman spectrum would remain relatively unchanged while the XRD pattern would decrease, as shown in our results.

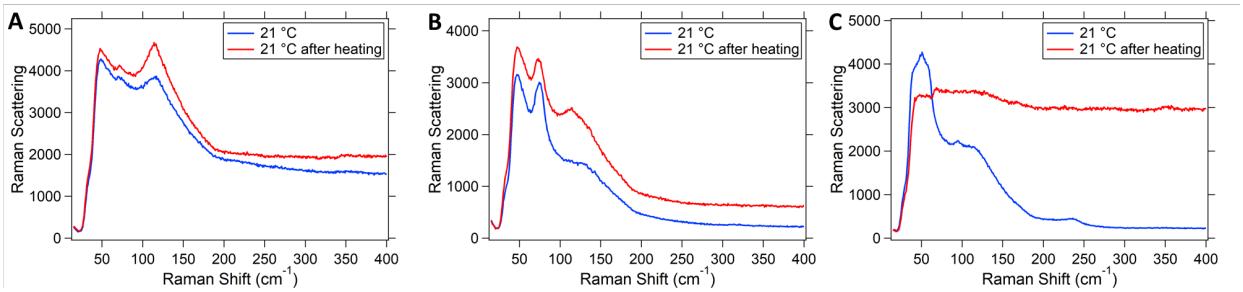

Figure 7. Raman spectra of A) $CsPbCl_3$, B) $CsPbBr_3$, and C) $CsPbI_3$ nanocrystals before and after heating to 250 °C and allowing the samples to cool.

Single crystal luminescence movies could not be collected during heating cycles due to instrument limitations, so solution-phase fluorescence spectra were acquired to observe the effect of temperature on the luminescence band for $CsPbX_3$ nanocrystals (**Figure S7**). In general, an increase in temperature leads to luminescence quenching when the thermal (kT) energy approaches the trap state energy.[51] We observe this as well (by comparing the SNR of normalized spectra), along with slight shifts in the luminescence maximum. The $CsPbCl_3$ sample shows a slight red shift as temperature is increased, which appears to be partially reversible after cooling back to room temperature. For $CsPbBr_3$ and $CsPbI_3$, slight blue shifts are observed with heating, however, $CsPbBr_3$ does not shift back upon cooling, indicating an irreversible process occurred. In contrast, $CsPbI_3$ completely recovers the original luminescence maximum. Irreversible processes typically involve changes within the material, while reversible processes involve changes to surface states.[51]

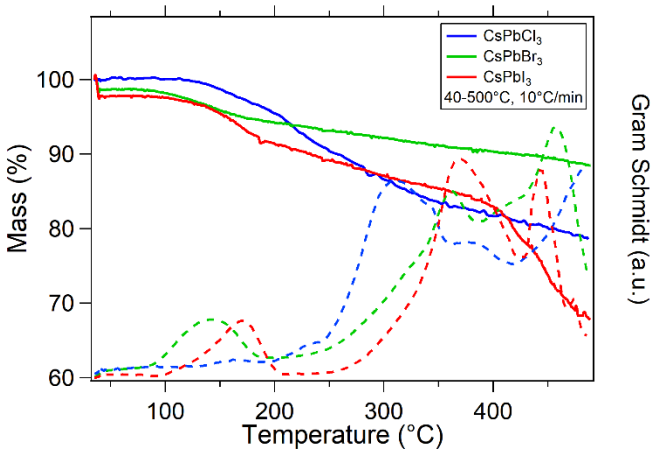

Figure 8. TGA-FTIR Mass loss and Gram-Schmidt curves for $CsPbX_3$ nanocrystals from 40-500 °C. The Gram-Schmidt curves monitor the total change in FTIR signal over time, indicating FTIR detection of mass loss products.

The thermal decomposition products were further analyzed with TGA-FTIR measurements and the results are shown in **Figure 8**. In addition to mass loss plots, the Gram-Schmidt curves for each sample are shown as well, which represent the total change in the FTIR signal based on successive measurements. In all samples, the mass loss from roughly 100-200 °C corresponded with oleylamine and oleic acid surface ligands, while the rest of the mass loss above 250 °C is due to CO_2, which can be from reaction and breakdown of the surface ligands with the O_2 from the 80% N_2 and 20% O_2 gas flow used in these measurements. Though octadecene is present in the reaction as well, it has been shown that oleic acid and oleylamine are the binding surface ligands, and the chemistry at the surface of these crystals is dynamic and cooperative.[75-76] These results are similar to recent reports showing TGA measurements of $CsPbI_3$,[74] $CsPbBr_3$,[77] and Mn^{2+}-doped $CsPbCl_3$.[30] In the case of $CsPbI_3$, the previous report indicates the bulk material begins to degrade above 400 °C, which helps explain the rapid mass loss we observed for nanocrystals of the same composition. Representative FTIR spectra (**Figure S8)** show the surface ligands and CO_2 signal measured at selected temperatures. In all cases, no gaseous loss products are detected that contain cesium, lead, or the halide species.

Conclusions

The halide composition of the $CsPbX_3$ nanocrystals has a significant effect on their stability. While exhibiting bright luminescence and good photostability, $CsPbI_3$-MeOAc nanocrystals are the most prone to degradation under heating. $CsPbI_3$ nanocrystals exhibit the most stable photophysical states by single crystal luminescence analysis, but eventually degrade under light and readily degrade under heating. $CsPbBr_3$ nanocrystals are the most resilient to degradation, though the photophysical states appear to change based on single crystal luminescence analysis during illumination in ambient conditions, which does represent photo-instability. $CsPbCl_3$ showed good stability under illumination and at elevated temperature, with possible crystal growth or orientation effects observed during illumination. While the smaller $CsPbI_3$-MeOAc nanocrystals show improved photostability compared to larger $CsPbI_3$ nanocrystals, it is also possible that surface chemistry differences in these two samples produce some or all of this effect. Additional experiments will be informative in unravelling which has the more dominant effect. Substituting Cs^+ in place of the methylammonium cation improves the stability for all compositions based on a comparison to published data,[7] although surface protection or encapsulation is still necessary for long-term downstream applications of $CsPbX_3$ nanocrystals in high-light-irradiance or elevated temperature environments.

Experimental Section

Materials

Lead chloride ($PbCl_2$, 99%), lead bromide ($PbBr_2$, 99%), lead iodide (PbI_2, 99%), 1-octadecene (ODE, 90%), oleic acid (OA, 90%), oleylamine (OLA, 80-90%), and cesium carbonate (Cs_2CO_3, 99.9%) were purchased from Sigma Aldrich.

Preparation of the Nanocrystals

$CsPbX_3$ nanocrystals were synthesized using a modified literature procedure.[15] Briefly, PbX_2 (0.188 mol), $PbCl_2$ (0.087 g), $PbBr_2$ (0.069 g), PbI_2 (0.052 g), was added to an oven-dry three-neck 250 mL flask containing ODE (5 mL), oleic acid (0.5 mL), and oleylamine (0.5 mL). The contents were degassed at 80 °C for 1 h and the flask was refilled with Ar and heated to 150 °C. A Cs-oleate solution (0.4 mL, 0.125 M in ODE) prepared by dissolving Cs_2CO_3 (2.49 mmol, 0.814g) in 40 mL of ODE was quickly injected, and 5 s later the reaction mixture was cooled by an ice-water bath. The nanocrystals were purified by crashing two times with 1:1 (v/v) acetone/methanol solution and centrifugation at 4500 rpm for 5 min followed by redispersion in 5 mL of toluene. In the case of $CsPbI_3$, purification was also carried out using methyl acetate in order to generate smaller nanocrystals, following the work of Swarnkar *et al*,[59] subsequently referred to as $CsPbI_3$-MeOAc.

Transmission electron microscopy (TEM) was performed using a Tecnai G2 F20 field emission TEM instrument (FEI, Hillsboro, OR) operating at ≤200 kV. Samples were prepared by placing 1 or 2 drops of concentrated toluene solutions onto carbon-coated copper grids. Powder X-ray diffraction (XRD) was measured using Cu Kα radiation on an Ultima IV diffractometer (Rigaku, The Woodlands, TX). The scanning range was 10-60° 2θ, with a step size of 0.02°.

Optical Characterization

Solution extinction (absorption plus scattering) spectra were measured using a photodiode array 8453 UV-Vis spectrophotometer (Agilent, Santa Clara, CA). Steady-state

photoluminescence (PL) spectra were measured using a Nanolog scanning spectrofluorometer (HORIBA Scientific, Edison, NJ) equipped with a liquid nitrogen-cooled InGaAs photodiode array. The excitation wavelength was 350 nm for $CsPbCl_3$ and $CsPbBr_3$, and 500 nm for $CsPbI_3$.

Single crystal photoluminescence movies were recorded on an Eclipse 80*i* upright microscope (Nikon Instruments, Melville, NY) fitted with a 100× (1.49 NA) oil immersion objective. An Xcite 120 PC mercury lamp was used for excitation (EXPO Photonic Solutions, Quebec City, Quebec, Canada). The nanocrystals were diluted 1:100 and sonicated for 60 min prior to drop casting onto glass microscope coverslips (Electron Microscopy Sciences, Hatfield, PA). 500 ± 10 nm excitation and 535 ± 15 nm emission filters were used for $CsPbBr_3$, and 510 ± 10 nm excitation and 731 ± 70 nm emission filters were used for $CsPbI_3$. The epi-luminescence was detected by an Evolve EMCCD camera (Photometrics, Tuscon, AZ). PL movies were collected with an acquisition time of 20 ms and a length of 2000 frames, and factoring in readout time the total analysis time was 60 s. The EM gain settings for each sample type were 20× ($CsPbBr_3$), and 1× ($CsPbI_3$), and 5 movies of each sample type were recorded.

Raman microspectroscopy was performed on nanocrystals using an XploRA Plus confocal Raman microscope (HORIBA Scientific, Edison, NJ) fitted with a 100× (0.90 NA) objective. The samples were drop cast onto glass slides and dried under ambient conditions. A 785-nm laser operating at 0.8 mW (~2×10^4 W/cm^2) was used for excitation with an edge filter, allowing for data collection down to 40 cm^{-1}. Two accumulations of 60 s each were acquired to exclude cosmic rays. The data were plotted using IGOR 6.37 (WaveMetrics, Portland, OR).

Photostability Study

To assess the photostability of the nanocrystals, a model 10500 compact solar simulator lamp (Abet Technologies, Milford, CT) was used to illuminate drop cast nanocrystal samples. At

intervals, Raman spectra and XRD patterns were collected on full-concentration samples, while single crystal luminescence movies and luminescence spectra were collected on 1:100 diluted samples to observe signs of degradation. All measurements were carried out using conditions outlined above.

Thermal Stability Study

For thermal stability measurements, 10 μL of the nanocrystal samples was drop cast onto cover glass and was allowed to dry for 30 min. A THMS600 temperature stage equipped with a LNP95 liquid nitrogen pump (Linkam Scientific Instruments, Tadworth, UK) was used to heat the samples after purging with nitrogen, using a ramp rate of 40 °C/min and allowing 30 min stabilization time for temperature changes. For Raman spectra, a 50× (0.5 NA) long working distance objective was used, acquiring spectra at room temperature, then 250 °C, then after cooling back to room temperature. XRD patterns were collected for samples heated to 50, 100, and 250 °C with stabilization periods of 5 min after being resuspended in toluene and drop casted onto a silicon XRD sample holder.

Thermogravimetric analysis coupled with FTIR (TGA-FTIR) was performed on an STA449F1 TGA/DSC System (Netzsch, Selb, Germany) using Al_2O_3 crucibles. The temperature program was an isothermal step at 40 °C for 5 min followed by a 10 °C/min ramp from 40-500 °C. The purge gases were set to 10 mL/min high purity N_2, 10 mL/min high-purity O_2, and 30 mL/min high-purity N_2 on the protective line to simulate air while maintaining low residual H_2O in the furnace. The system was coupled to a Tensor 10 FTIR (Bruker, Billerica, MA) equipped with a TGA-IR temperature controlled 10 cm lightpipe sample stage set to 200 °C, and transfer lines were also kept at 200 °C. 1-2 mg of nanocrystals were deposited in the crucibles for analysis.

Supporting Information

Additional experimental details, Time-correlated photoluminescence, representative photoluminescence movies, plots of luminescence types, counting statistics for photoluminescence types, fit parameters for ON-OFF histogram analysis, Raman spectra of nanocrystals following solar simulator exposure, and representative FTIR spectra from TGA-FTIR are available free of charge from the *ChemPhysChem* home page (https://onlinelibrary.wiley.com/journal/14397641).

Acknowledgements

This research is supported by the U.S. Department of Energy, Office of Basic Energy Sciences, Division of Chemical Sciences, Geosciences, and Biosciences through the Ames Laboratory. Electron microscopy characterization was performed at Ames Laboratory's Sensitive Instrument Facility. Ames Laboratory is operated for the U.S. Department of Energy by Iowa State University under contract # DE-AC02-07CH11358.

References

[1] Akkerman, Q. A.; Rainò, G.; Kovalenko, M. V.; Manna, L., Genesis, Challenges and Opportunities for Colloidal Lead Halide Perovskite Nanocrystals. *Nature Materials* **2018,** *17*, 394-405.

[2] Correa-Baena, J.-P.; Abate, A.; Saliba, M.; Tress, W.; Jacobsson, T. J.; Grätzel, M.; Hagfeldt, A., The Rapid Evolution of Highly Efficient Perovskite Solar Cells. *Energy & Environmental Science* **2017,** *10* (3), 710-727.

[3] Swarnkar, A.; Ravi, V. K.; Nag, A., Beyond Colloidal Cesium Lead Halide Perovskite Nanocrystals: Analogous Metal Halides and Doping. *ACS Energy Letters* **2017,** *2* (5), 1089-1098.

[4] Yang, D.; Cao, M.; Zhong, Q.; Li, P.; Zhang, X.; Zhang, Q., All-inorganic cesium lead halide perovskite nanocrystals: synthesis, surface engineering and applications. *Journal of Materials Chemistry C* **2019,** *7* (4), 757-789.

[5] Bryant, D.; Aristidou, N.; Pont, S.; Sanchez-Molina, I.; Chotchunangatchaval, T.; Wheeler, S.; Durrant, J. R.; Haque, S. A., Light and Oxygen Induced Degradation Limits the Operational Stability of Methylammonium Lead Triiodide Perovskite Solar Cells. *Energy & Environmental Science* **2016,** *9* (5), 1655-1660.

[6] Beal, R. E.; Slotcavage, D. J.; Leijtens, T.; Bowring, A. R.; Belisle, R. A.; Nguyen, W. H.; Burkhard, G. F.; Hoke, E. T.; McGehee, M. D., Cesium Lead Halide Perovskites With Improved Stability for Tandem Solar Cells. *The Journal of Physical Chemistry Letters* **2016,** *7* (5), 746-751.

[7] Kulbak, M.; Gupta, S.; Kedem, N.; Levine, I.; Bendikov, T.; Hodes, G.; Cahen, D., Cesium Enhances Long-term Stability of Lead Bromide Perovskite-based Solar Cells. *The Journal of Physical Chemistry Letters* **2015,** *7* (1), 167-172.

[8] Sutton, R. J.; Eperon, G. E.; Miranda, L.; Parrott, E. S.; Kamino, B. A.; Patel, J. B.; Hörantner, M. T.; Johnston, M. B.; Haghighirad, A. A.; Moore, D. T., Bandgap- Tunable Cesium Lead Halide Perovskites with High Thermal Stability for Efficient Solar Cells. *Advanced Energy Materials* **2016,** *6* (8), 1502458.

[9] Sanehira, E. M.; Marshall, A. R.; Christians, J. A.; Harvey, S. P.; Ciesielski, P. N.; Wheeler, L. M.; Schulz, P.; Lin, L. Y.; Beard, M. C.; Luther, J. M., Enhanced Mobility $CsPbI_3$

Quantum Dot Arrays for Record-Efficiency, High-Voltage Photovoltaic Cells. *Science Advances* **2017,** *3* (10), eaao4204.

[10] Wang, K.; Jin, Z.; Liang, L.; Bian, H.; Bai, D.; Wang, H.; Zhang, J.; Wang, Q.; Liu, S., All-inorganic cesium lead iodide perovskite solar cells with stabilized efficiency beyond 15%. *Nature Communications* **2018,** *9* (1), 4544.

[11] Eaton, S. W.; Lai, M.; Gibson, N. A.; Wong, A. B.; Dou, L.; Ma, J.; Wang, L.-W.; Leone, S. R.; Yang, P., Lasing in Robust Cesium Lead Halide Perovskite Nanowires. *Proceedings of the National Academy of Sciences* **2016,** *113* (8), 1993-1998.

[12] Wang, S.; Wang, K.; Gu, Z.; Wang, Y.; Huang, C.; Yi, N.; Xiao, S.; Song, Q., Solution-Phase Synthesis of Cesium Lead Halide Perovskite Microrods for High- Quality Microlasers and Photodetectors. *Advanced Optical Materials* **2017,** *5* (11), 1700023.

[13] Wang, X.; Shoaib, M.; Wang, X.; Zhang, X.; He, M.; Luo, Z.; Zheng, W.; Li, H.; Yang, T.; Zhu, X., High-Quality In-Plane Aligned $CsPbX_3$ Perovskite Nanowire Lasers with Composition Dependent Strong Exciton-Photon Coupling. *ACS Nano* **2018,** *12* (6), 6170–6178.

[14] Evans, T. J.; Schlaus, A.; Fu, Y.; Zhong, X.; Atallah, T. L.; Spencer, M. S.; Brus, L. E.; Jin, S.; Zhu, X. Y., Continuous- Wave Lasing in Cesium Lead Bromide Perovskite Nanowires. *Advanced Optical Materials* **2018,** *6* (2), 1700982.

[15] Protesescu, L.; Yakunin, S.; Bodnarchuk, M. I.; Krieg, F.; Caputo, R.; Hendon, C. H.; Yang, R. X.; Walsh, A.; Kovalenko, M. V., Nanocrystals of Cesium Lead Halide Perovskites ($CsPbX_3$, X= Cl, Br, and I): Novel Optoelectronic Materials Showing Bright Emission with Wide Color Gamut. *Nano Letters* **2015,** *15* (6), 3692-3696.

[16] Song, J.; Li, J.; Li, X.; Xu, L.; Dong, Y.; Zeng, H., Quantum Dot Light- Emitting Diodes Based on Inorganic Perovskite Cesium Lead Halides ($CsPbX_3$). *Advanced Materials* **2015,** *27* (44), 7162-7167.

[17] Lu, M.; Zhang, X.; Bai, X.; Wu, H.; Shen, X.; Zhang, Y.; Zhang, W.; Zheng, W.; Song, H.; Yu, W. W., Spontaneous Silver Doping and Surface Passivation of $CsPbI_3$ Perovskite Active Layer Enable Light-Emitting Devices with an External Quantum Efficiency of 11.2%. *ACS Energy Letters* **2018,** *3*, 1571-1577.

[18] Sheng, X.; Chen, G.; Wang, C.; Wang, W.; Hui, J.; Zhang, Q.; Yu, K.; Wei, W.; Yi, M.; Zhang, M., Polarized Optoelectronics of $CsPbX_3$ (X= Cl, Br, I) Perovskite Nanoplates with Tunable Size and Thickness. *Advanced Functional Materials* **2018,** *28* (19), 1800283.

[19] Ramasamy, P.; Lim, D.-H.; Kim, B.; Lee, S.-H.; Lee, M.-S.; Lee, J.-S., All-Inorganic Cesium Lead Halide Perovskite Nanocrystals for Photodetector Applications. *Chemical Communications* **2016,** *52* (10), 2067-2070.

[20] Lv, L.; Xu, Y.; Fang, H.; Luo, W.; Xu, F.; Liu, L.; Wang, B.; Zhang, X.; Yang, D.; Hu, W., Generalized Colloidal Synthesis of High-quality, Two-dimensional Cesium Lead Halide Perovskite Nanosheets and Their Applications in Photodetectors. *Nanoscale* **2016,** *8* (28), 13589-13596.

[21] Sun, S.; Yuan, D.; Xu, Y.; Wang, A.; Deng, Z., Ligand-Mediated Synthesis of Shape-Controlled Cesium Lead Halide Perovskite Nanocrystals via Reprecipitation Process at Room Temperature. *ACS Nano* **2016,** *10* (3), 3648-3657.

[22] Ye, S.; Zhao, M.; Song, J.; Qu, J., Controllable Emission Bands and Morphologies of High-Quality $CsPbX_3$ Perovskite Nanocrystals Prepared in Octane. *Nano Research* **2018,** *11* (9), 4654-4663.

[23] Zhang, D.; Eaton, S. W.; Yu, Y.; Dou, L.; Yang, P., Solution-Phase Synthesis of Cesium Lead Halide Perovskite Nanowires. *Journal of the American Chemical Society* **2015,** *137* (29), 9230-9233.

[24] Liu, F.; Zhang, Y.; Ding, C.; Kobayashi, S.; Izuishi, T.; Nakazawa, N.; Toyoda, T.; Ohta, T.; Hayase, S.; Minemoto, T., Highly Luminescent Phase-Stable $CsPbI_3$ Perovskite Quantum Dots Achieving Near 100% Absolute Photoluminescence Quantum Yield. *ACS Nano* **2017,** *11* (10), 10373-10383.

[25] Lu, C.; Li, H.; Kolodziejski, K.; Dun, C.; Huang, W.; Carroll, D.; Geyer, S. M., Enhanced stabilization of inorganic cesium lead triiodide (CsPbI 3) perovskite quantum dots with tri-octylphosphine. *Nano Research* **2018,** *11* (2), 762-768.

[26] Abdi-Jalebi, M.; Andaji-Garmaroudi, Z.; Cacovich, S.; Stavrakas, C.; Philippe, B.; Richter, J. M.; Alsari, M.; Booker, E. P.; Hutter, E. M.; Pearson, A. J., Maximizing and stabilizing luminescence from halide perovskites with potassium passivation. *Nature* **2018,** *555* (7697), 497.

[27] Ahmed, T.; Seth, S.; Samanta, A., Boosting the Photoluminescence of CsPbX3 (X= Cl, Br, I) Perovskite Nanocrystals Covering a Wide Wavelength Range by Postsynthetic Treatment with Tetrafluoroborate Salts. *Chemistry of Materials* **2018,** *30* (11), 3633-3637.

[28] Wang, S.; Wang, Y.; Zhang, Y.; Zhang, X.; Shen, X.; Zhuang, X.; Lu, P.; Yu, W. W.; Kershaw, S. V.; Rogach, A. L., Cesium Lead Chloride/Bromide Perovskite Quantum Dots with Strong Blue Emission Realized via a Nitrate-Induced Selective Surface Defect Elimination Process. *The journal of physical chemistry letters* **2018,** *10* (1), 90-96.

[29] Bohn, B. J.; Tong, Y.; Gramlich, M.; Lai, M. L.; Döblinger, M.; Wang, K.; Hoye, R. L.; Müller-Buschbaum, P.; Stranks, S. D.; Urban, A. S., Boosting tunable blue luminescence of

halide perovskite nanoplatelets through postsynthetic surface trap repair. *Nano letters* **2018,** *18* (8), 5231-5238.

[30] Mir, W. J.; Jagadeeswararao, M.; Das, S.; Nag, A., Colloidal Mn-doped Cesium Lead Halide Perovskite Nanoplatelets. *ACS Energy Letters* **2017,** *2* (3), 537-543.

[31] Parobek, D.; Dong, Y.; Qiao, T.; Rossi, D.; Son, D. H., Photoinduced Anion Exchange in Cesium Lead Halide Perovskite Nanocrystals. *Journal of the American Chemical Society* **2017,** *139* (12), 4358-4361.

[32] Parobek, D.; Roman, B. J.; Dong, Y.; Jin, H.; Lee, E.; Sheldon, M.; Son, D. H., Exciton-to-dopant Energy Transfer in Mn-doped Cesium Lead Halide Perovskite Nanocrystals. *Nano Letters* **2016,** *16* (12), 7376-7380.

[33] Zhu, J.; Yang, X.; Zhu, Y.; Wang, Y.; Cai, J.; Shen, J.; Sun, L.; Li, C., Room-Temperature Synthesis of Mn-Doped Cesium Lead Halide Quantum Dots with High Mn Substitution Ratio. *The Journal of Physical Chemistry Letters* **2017,** *8* (17), 4167-4171.

[34] Milstein, T.; Kroupa, D.; Gamelin, D. R., Picosecond Quantum Cutting Generates Photoluminescence Quantum Yields Over 100% in Ytterbium-Doped $CsPbCl_3$ Nanocrystals. *Nano Letters* **2018,** *18* (6), 3792–3799.

[35] Bi, C.; Wang, S.; Li, Q.; Kershaw, S. V.; Tian, J.; Rogach, A. L., Thermally Stable Copper (II) Doped Cesium Lead Halide Perovskite Quantum Dots with a Strong Blue Emission. *The journal of physical chemistry letters* **2019**.

[36] Akkerman, Q. A.; D'Innocenzo, V.; Accornero, S.; Scarpellini, A.; Petrozza, A.; Prato, M.; Manna, L., Tuning the Optical Properties of Cesium Lead Halide Perovskite Nanocrystals by Anion Exchange Reactions. *Journal of the American Chemical Society* **2015,** *137* (32), 10276-10281.

[37] Creutz, S. E.; Crites, E. N.; De Siena, M. C.; Gamelin, D. R., Colloidal Nanocrystals of Lead-Free Double-Perovskite (Elpasolite) Semiconductors: Synthesis and Anion Exchange to Access New Materials. *Nano Letters* **2018,** *18* (2), 1118-1123.

[38] Nedelcu, G.; Protesescu, L.; Yakunin, S.; Bodnarchuk, M. I.; Grotevent, M. J.; Kovalenko, M. V., Fast Anion-exchange in Highly Luminescent Nanocrystals of Cesium Lead Halide Perovskites ($CsPbX_3$, X= Cl, Br, I). *Nano Letters* **2015,** *15* (8), 5635-5640.

[39] Chen, Y.-C.; Chou, H.-L.; Lin, J.-C.; Lee, Y.-C.; Pao, C.-W.; Chen, J.-L.; Chang, C.-C.; Chi, R.-Y.; Kuo, T.-R.; Lu, C.-W., Enhanced Luminescence and Stability of Cesium Lead Halide Perovskite CsPbX3 Nanocrystals by Cu2+-Assisted Anion Exchange Reactions. *The Journal of Physical Chemistry C* **2019,** *123* (4), 2353-2360.

[40] Chen, L.; Tan, Y.-Y.; Chen, Z.-X.; Wang, T.; Hu, S.; Nan, Z.-A.; Xie, L.-Q.; Hui, Y.; Huang, J.-X.; Zhan, C., Toward Long-Term Stability: Single-Crystal Alloys of Cesium-Containing Mixed Cation and Mixed Halide Perovskite. *Journal of the American Chemical Society* **2019,** *141* (4), 1665-1671.

[41] Sum, T. C.; Mathews, N., Advancements in Perovskite Solar Cells: Photophysics Behind the Photovoltaics. *Energy & Environmental Science* **2014,** *7* (8), 2518-2534.

[42] Freppon, D. J.; Men, L.; Burkhow, S. J.; Petrich, J. W.; Vela, J.; Smith, E. A., Photophysical properties of wavelength-tunable methylammonium lead halide perovskite nanocrystals. *Journal of Materials Chemistry C* **2017,** *5* (1), 118-126.

[43] Zhu, F.; Men, L.; Guo, Y.; Zhu, Q.; Bhattacharjee, U.; Goodwin, P. M.; Petrich, J. W.; Smith, E. A.; Vela, J., Shape Evolution and Single Particle Luminescence of Organometal Halide Perovskite Nanocrystals. *ACS Nano* **2015,** *9* (3), 2948-2959.

[44] Luo, L.; Men, L.; Liu, Z.; Mudryk, Y.; Zhao, X.; Yao, Y.; Park, J. M.; Shinar, R.; Shinar, J.; Ho, K.-M., Ultrafast Terahertz Snapshots of Excitonic Rydberg States and Electronic Coherence in an Organometal Halide Perovskite. *Nature Communications* **2017,** *8*, 15565.

[45] Yuan, H.; Debroye, E.; Caliandro, G.; Janssen, K. P.; Van Loon, J.; Kirschhock, C. E.; Martens, J. A.; Hofkens, J.; Roeffaers, M. B., Photoluminescence Blinking of Single-Crystal Methylammonium Lead Iodide Perovskite Nanorods Induced by Surface Traps. *ACS Omega* **2016,** *1* (1), 148-159.

[46] Tian, Y.; Merdasa, A.; Peter, M.; Abdellah, M.; Zheng, K.; Ponseca, C. S., Jr.; Pullerits, T.; Yartsev, A.; Sundstrom, V.; Scheblykin, I. G., Giant photoluminescence blinking of perovskite nanocrystals reveals single-trap control of luminescence. *Nano Lett* **2015,** *15* (3), 1603-8.

[47] Galland, C.; Ghosh, Y.; Steinbruck, A.; Sykora, M.; Hollingsworth, J. A.; Klimov, V. I.; Htoon, H., Two types of luminescence blinking revealed by spectroelectrochemistry of single quantum dots. *Nature* **2011,** *479* (7372), 203-7.

[48] Srimath Kandada, A. R.; Petrozza, A., Photophysics of Hybrid Lead Halide Perovskites: The Role of Microstructure. *Acc Chem Res* **2016,** *49* (3), 536-44.

[49] Zhao, P.; Xu, J.; Dong, X.; Wang, L.; Ren, W.; Bian, L.; Chang, A., Large-Size CH3NH3PbBr3 Single Crystal: Growth and In Situ Characterization of the Photophysics Properties. *J Phys Chem Lett* **2015,** *6* (13), 2622-8.

[50] Fang, H.-H.; Raissa, R.; Abdu-Aguye, M.; Adjokatse, S.; Blake, G. R.; Even, J.; Loi, M. A., Photophysics of Organic-Inorganic Hybrid Lead Iodide Perovskite Single Crystals. *Advanced Functional Materials* **2015,** *25* (16), 2378-2385.

[51] Diroll, B. T.; Nedelcu, G.; Kovalenko, M. V.; Schaller, R. D., High- Temperature Photoluminescence of $CsPbX_3$ (X= Cl, Br, I) Nanocrystals. *Advanced Functional Materials* **2017,** *27* (21).

[52] Park, Y.-S.; Guo, S.; Makarov, N. S.; Klimov, V. I., Room Temperature Single-Photon Emission From Individual Perovskite Quantum Dots. *ACS Nano* **2015,** *9* (10), 10386-10393.

[53] Rainò, G.; Nedelcu, G.; Protesescu, L.; Bodnarchuk, M. I.; Kovalenko, M. V.; Mahrt, R. F.; Stöferle, T., Single Cesium Lead Halide Perovskite Nanocrystals at Low Temperature: Fast Single-Photon Emission, Reduced Blinking, and Exciton Fine Structure. *ACS Nano* **2016,** *10* (2), 2485-2490.

[54] Yuan, G. c.; Ritchie, C.; Ritter, M.; Murphy, S.; Gómez, D. E.; Mulvaney, P., The Degradation and Blinking of Single Perovskite Quantum Dots. *The Journal of Physical Chemistry C* **2018,** *122* (25), 13407–13415.

[55] Becker, M. A.; Vaxenburg, R.; Nedelcu, G.; Sercel, P. C.; Shabaev, A.; Mehl, M. J.; Michopoulos, J. G.; Lambrakos, S. G.; Bernstein, N.; Lyons, J. L., Bright triplet excitons in caesium lead halide perovskites. *Nature* **2018,** *553* (7687), 189.

[56] Pan, G.; Bai, X.; Yang, D.; Chen, X.; Jing, P.; Qu, S.; Zhang, L.; Zhou, D.; Zhu, J.; Xu, W., Doping Lanthanide into Perovskite Nanocrystals: Highly Improved and Expanded Optical Properties. *Nano Letters* **2017,** *17* (12), 8005-8011.

[57] Yuan, X.; Ji, S.; De Siena, M. C.; Fei, L.; Zhao, Z.; Wang, Y.; Li, H.; Zhao, J.; Gamelin, D. R., Photoluminescence Temperature Dependence, Dynamics, and Quantum Efficiencies in Mn^{2+}-Doped $CsPbCl_3$ Perovskite Nanocrystals with Varied Dopant Concentration. *Chemistry of Materials* **2017,** *29* (18), 8003-8011.

[58] Beimborn, J. C.; Hall, L. M.; Tongying, P.; Dukovic, G.; Weber, J. M., Pressure Response of Photoluminescence in Cesium Lead Iodide Perovskite Nanocrystals. *The Journal of Physical Chemistry C* **2018,** *122* (20), 11024-11030.

[59] Swarnkar, A.; Marshall, A. R.; Sanehira, E. M.; Chernomordik, B. D.; Moore, D. T.; Christians, J. A.; Chakrabarti, T.; Luther, J. M., Quantum Dot–Induced Phase Stabilization of α-CsPbI3 Perovskite for High-Efficiency Photovoltaics. *Science* **2016,** *354* (6308), 92-95.

[60] Hai, J.; Li, H.; Zhao, Y.; Chen, F.; Peng, Y.; Wang, B., Designing of Blue, Green, and Red $CsPbX_3$ Perovskite-Codoped Flexible Films with Water Resistant Property and Elimination of Anion-Exchange for Tunable White Light Emission. *Chemical Communications* **2017,** *53* (39), 5400-5403.

[61] Demkiv, T.; Myagkota, S.; Malyi, T.; Pushak, A.; Vistovskyy, V.; Yakibchuk, P.; Shapoval, O.; Mitina, N.; Zaichenko, A.; Voloshinovskii, A., Luminescence Properties of $CsPbBr_3$ Nanocrystals Dispersed in a Polymer Matrix. *Journal of Luminescence* **2018,** *198*, 103-107.

[62] Pan, A.; Jurow, M. J.; Qiu, F.; Yang, J.; Ren, B.; Urban, J. J.; He, L.; Liu, Y., Nanorod Suprastructures from a Ternary Graphene Oxide–Polymer–$CsPbX_3$ Perovskite Nanocrystal Composite That Display High Environmental Stability. *Nano Letters* **2017,** *17* (11), 6759-6765.

[63] Yoon, H. C.; Lee, S.; Song, J. K.; Yang, H.; Do, Y. R., Efficient and Stable $CsPbBr_3$ Quantum-Dot Powders Passivated and Encapsulated with a Mixed Silicon Nitride and Silicon Oxide Inorganic Polymer Matrix. *ACS Applied Materials & Interfaces* **2018,** *10* (14), 11756-11767.

[64] Krieg, F.; Ochsenbein, S. T.; Yakunin, S.; Ten Brinck, S.; Aellen, P.; Süess, A.; Clerc, B.; Guggisberg, D.; Nazarenko, O.; Shynkarenko, Y., Colloidal $CsPbX_3$ (X= Cl, Br, I)

Nanocrystals 2.0: Zwitterionic Capping Ligands for Improved Durability and Stability. *ACS Energy Letters* **2018,** *3* (3), 641-646.

[65] Li, H.; Qian, Y.; Xing, X.; Zhu, J.; Huang, X.; Jing, Q.; Zhang, W.; Zhang, C.; Lu, Z., Enhancing Luminescence and Photostability of $CsPbBr_3$ Nanocrystals via Surface Passivation with Silver Complex. *The Journal of Physical Chemistry C* **2018,** *122* (24), 12994-13000.

[66] Liao, M.; Shan, B.; Li, M., In Situ Raman Spectroscopic Studies of Thermal Stability of All-Inorganic Cesium Lead Halide (CsPbX3, X= Cl, Br, I) Perovskite Nanocrystals. *The journal of physical chemistry letters* **2019,** *10*, 1217-1225.

[67] Christians, J. A.; Schulz, P.; Tinkham, J. S.; Schloemer, T. H.; Harvey, S. P.; de Villers, B. J. T.; Sellinger, A.; Berry, J. J.; Luther, J. M., Tailored interfaces of unencapsulated perovskite solar cells for> 1,000 hour operational stability. *Nature Energy* **2018,** *3* (1), 68.

[68] Bertolotti, F.; Protesescu, L.; Kovalenko, M. V.; Yakunin, S.; Cervellino, A.; Billinge, S. J.; Terban, M. W.; Pedersen, J. S.; Masciocchi, N.; Guagliardi, A., Coherent Nanotwins and Dynamic Disorder in Cesium Lead Halide Perovskite Nanocrystals. *ACS Nano* **2017,** *11* (4), 3819-3831.

[69] Cottingham, P.; Brutchey, R. L., On the Crystal Structure of Colloidally Prepared $CsPbBr_3$ Quantum Dots. *Chemical Communications* **2016,** *52* (30), 5246-5249.

[70] Bekenstein, Y.; Koscher, B. A.; Eaton, S. W.; Yang, P.; Alivisatos, A. P., Highly Luminescent Colloidal Nanoplates of Perovskite Cesium Lead Halide and Their Oriented Assemblies. *Journal of the American Chemical Society* **2015,** *137* (51), 16008-16011.

[71] Santra, K.; Zhan, J.; Song, X.; Smith, E. A.; Vaswani, N.; Petrich, J. W., What Is the Best Method to Fit Time-Resolved Data? A Comparison of the Residual Minimization and the

Maximum Likelihood Techniques as Applied to Experimental Time-Correlated, Single-Photon Counting Data. *The Journal of Physical Chemistry B* **2016,** *120* (9), 2484-2490.

[72] Yaffe, O.; Guo, Y.; Tan, L. Z.; Egger, D. A.; Hull, T.; Stoumpos, C. C.; Zheng, F.; Heinz, T. F.; Kronik, L.; Kanatzidis, M. G., Local Polar Fluctuations in Lead Halide Perovskite Crystals. *Physical Review Letters* **2017,** *118* (13), 136001.

[73] Stoumpos, C. C.; Malliakas, C. D.; Kanatzidis, M. G., Semiconducting Tin and Lead Iodide Perovskites with Organic Cations: Phase Transitions, High Mobilities, and Near-Infrared Photoluminescent Properties. *Inorganic Chemistry* **2013,** *52* (15), 9019-9038.

[74] Dastidar, S.; Hawley, C. J.; Dillon, A. D.; Gutierrez-Perez, A. D.; Spanier, J. E.; Fafarman, A. T., Quantitative Phase-Change Thermodynamics and Metastability of Perovskite-Phase Cesium Lead Iodide. *The Journal of Physical Chemistry Letters* **2017,** *8* (6), 1278-1282.

[75] De Roo, J.; Ibáñez, M.; Geiregat, P.; Nedelcu, G.; Walravens, W.; Maes, J.; Martins, J. C.; Van Driessche, I.; Kovalenko, M. V.; Hens, Z., Highly Dynamic Ligand Binding and Light Absorption Coefficient of Cesium Lead Bromide Perovskite Nanocrystals. *ACS Nano* **2016,** *10* (2), 2071-2081.

[76] Smock, S. R.; Williams, T. J.; Brutchey, R. L., Quantifying the Thermodynamics of Ligand Binding to $CsPbBr_3$ Quantum Dots. *Angewandte Chemie* **2018,** *130* (26), 11885-11889.

[77] Hoffman, J. B.; Zaiats, G.; Wappes, I.; Kamat, P. V., $CsPbBr_3$ Solar Cells: Controlled Film Growth through Layer-by-Layer Quantum Dot Deposition. *Chemistry of Materials* **2017,** *29* (22), 9767-9774.